Int. J. Heat Mass Transfer. Vol. 16, pp. 735–745. Pergamon Press 1973. Printed in Great Britain

THERMAL BUOYANCY IN ROUND LAMINAR VERTICAL JETS

J. C. MOLLENDORF
Engineering Research Center, Western Electric Company, Inc., Princeton, New Jersey 08540, U.S.A.
and
B. GEBHART
Sibley School of Mechanical Engineering, Upson Hall, Cornell University, Ithaca, New York 14850, U.S.A.

(*Received* 24 *February* 1972 *and in revised form* 5 *July* 1972)

Abstract—A perturbation analysis is performed which includes the effect of a small amount of thermal buoyancy on the velocity and temperature fields of a round, laminar, vertical jet. A numerical solution of the resulting perturbation equations shows that the predominant effect of positive thermal buoyancy is to increase the axial velocity component of the jet. The magnitude of the effect is shown to increase for decreasing Prandtl numbers. Other details of buoyancy effects on the flow and temperature fields are presented and discussed. It is expected that buoyancy effects may have a large influence on laminar stability.

INTRODUCTION

FLOWS commonly referred to as jets may be regarded as a part of a more general category of flows characterized by the absence of rigid boundaries. These "free boundary" flows include such things as jets, wakes, plumes, and thermals. It is convenient to further subdivide these flows on the basis of whether they are laminar or turbulent, and/or buoyant or nonbuoyant. There are a nearly unlimited number of important physical examples of these types of flows. Such flows are important in technology, meteorology, oceanography, air and water pollution etc. A few more specific examples are associated with the mechanics of cloud formation and cloud top oscillation, buoyancy driven ocean circulations, and the thermal circulation in lakes, resulting perhaps from water discharges. The purpose of this work is to determine the effect of thermal buoyancy on the velocity and temperature fields of a round laminar vertical jet.

The first important study recorded in the literature was Schlichting's [1] solution of the laminar jet in 1933. Using boundary layer approximations, similarity solutions were found for both the two-dimensional and axisymmetric jets. A closed form solution was presented for the axisymmetric case. Later Bickley [2] published a closed form solution for the two-dimensional case. Schlichting had also found this solution shortly after the publication of [1]. Results of these analyses showed that axial velocities decay as $x^{-\frac{1}{2}}$ and x^{-1} for the two-dimensional and axially symmetric jets respectively, and that the mass flow rates increase as $x^{\frac{1}{2}}$ and x, respectively. Note here that x is the coordinate along the axis of the jet, measured from its origin.

In 1937 Andrade and Tsien [3] experimentally verified Schlichting's results. They used a small (0·040 in.) diameter jet propelled by a hydrostatic head. The flow was observed optically by using suspended aluminum particles over the Reynolds number range from 50 to 300 (calculated from conditions at the nozzle) and the results agreed well with Schlichting's solution. Similar experiments with two-dimensional jets [4] proved to be less successful mainly because of the tendency of the jet to twist and assume a non-two-dimensional form.

The solution for a round laminar jet by Landdau [5] in 1943 is also important as one of the few exact solutions of the complete Navier–Stokes equations. This solution does not rely on

boundary layer simplifications. A spherical polar coordinate system is used and a similarity solution (in the usual sense) is found that results in closed form expressions for the velocity field. By using a series expansion involving the angle of spread, it can be shown that this solution becomes equivalent to that using boundary layer approximations for Reynolds numbers greater than 8.

Eight years after Landau's [5] results were presented, Squire [6] published an identical analysis. Squire [6] also presented a temperature solution neglecting the effects of buoyancy. It can be shown that this temperature solution also reduces to the boundary layer result at sufficiently large Reynolds numbers.

A paper in 1967 by Brand and Lahey [7] repeats various known point and line source plume solutions and attempts to relate plume and jet flows. The usefulness of the results is not apparent. The chosen matching conditions are that the jet velocity and temperature profiles match (in an average sense) a particular known plume flow at some location.

Although certain gross aspects of buoyancy have been observed by Vignes [8], there have been no experiments dealing directly with the effects of buoyancy on the details of the velocity and temperature profiles of laminar jets. There have, however, been several experiments [9–11] concerned with the transition of laminar jets to turbulence. Some of these may have been significantly influenced by buoyancy effects. McNaughton and Sinclair [9] state that small density differences between the inlet solution and the fluid in the vessel considerably affected the behavior of the jets. Marsters [10] calculated Gr/Re^2 to be 2×10^{-4} for his experiments and concluded that buoyant effects on his data are small. The work of McKenzie and Wall [11] lacks adequate documentation but it appears that the jets considered may have actually been quite buoyant. The relevant question in these studies may have actually been the effect of buoyancy on the hydrodynamic stability of a laminar jet.

ANALYSIS

We begin by presenting the full set of governing equations, apply the appropriate approximations, and review the known, non-buoyant, closed-form similarity solution. The effect of buoyancy is then included as a linear perturbation of the non-buoyant solution. The perturbation parameter is determined and the numerical procedure for integrating the resulting first order equations is discussed.

Consider the axisymmetric geometry of Fig. 1.

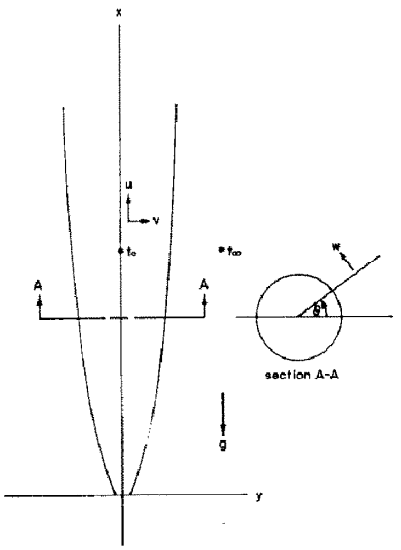

FIG. 1. Cylindrical coordinate system for axisymmetric jet.

Assuming that the flow is incompressible and neglecting viscous dissipation, the equations expressing the conservation of mass, momentum and energy for constant fluid properties are:

$$\nabla \cdot V = 0 \tag{1}$$

$$\rho\left[\frac{\partial V}{\partial \tau} + (V \cdot \nabla)V\right] = \rho g - \nabla p + \mu \nabla^2 V \tag{2}$$

$$\rho c_2\left[\frac{\partial t}{\partial \tau} + (V \cdot \nabla)t\right] = k\nabla^2 t. \tag{3}$$

Considering steady ($\partial/\partial\tau = 0$), axisymmetric ($\partial/\partial\theta = 0$) flow, with no swirl ($w = 0$); and applying the suitable boundary layer and

Boussinesq approximations, these equations become:

$$\frac{\partial}{\partial x}(yu) + \frac{\partial}{\partial y}(yv) = 0 \tag{4}$$

$$u\frac{\partial u}{\partial x} + v\frac{\partial u}{\partial y} = \nu\frac{1}{y}\frac{\partial}{\partial y}\left(y\frac{\partial u}{\partial y}\right) + g\beta(t - t_\infty) \tag{5}$$

$$u\frac{\partial t}{\partial x} + v\frac{\partial t}{\partial y} = \alpha\frac{1}{y}\frac{\partial}{\partial y}\left(y\frac{\partial t}{\partial y}\right). \tag{6}$$

These express the conservation of mass, x-direction force-momentum and energy. They describe the behavior of an axisymmetric, laminar, buoyant jet issuing into a quiescent, infinite medium at t_∞. The following boundary conditions are satisfied, where t_0 is the centerline temperature distribution.

at

$$y = 0: \qquad v = 0, \qquad \frac{\partial u}{\partial y} = 0, \qquad t = t_0$$

as (7)

$$y \to \infty: \qquad u \to 0, \qquad t \to t_\infty.$$

In 1933, H. Schlichting [1] neglected the buoyancy force term in (5) and found a closed form similarity solution which satisfies (4) and (5) and the velocity conditions of (7). The compatibility condition for a non-buoyant jet is that the momentum flux in the x direction be constant, i.e.

$$J \equiv \int_0^\infty 2\pi\rho u^2 y \, dy = \text{constant}. \tag{8}$$

As will be seen later, this condition is used to determine a constant arising from the integration of the momentum equation. Note that equation (8) will not be satisfied when the effect of buoyancy is included.

Although we will eventually include thermal buoyancy, it is convenient to first sketch a solution equivalent to that of [1].

These results will form the basis for the perturbation method of the next section which includes the effects of thermal buoyancy. The compatibility condition that the thermal energy convected be independent of x is written as follows.

$$Q \equiv \int_0^\infty 2\pi\rho c_p(t - t_\infty) uy \, dy = \text{constant}. \tag{9}$$

This condition applies whether or not the jet is considered buoyant.

The analysis proceeds through a consideration of conditions for similarity. The continuity equation is identically satisfied by defining a Stokes stream function as follows:

$$u \equiv \frac{v}{y}\psi_y \qquad \text{and} \qquad v \equiv -\frac{v}{y}\psi_x. \tag{10}$$

Forms for the similarity variable η, stream function ψ, and centerline temperature distribution d, are assumed in terms of unknown functions $b(x)$, $c(x)$, $d(x)$ as follows:

$$\eta = yb(x)/\sqrt{K}, \qquad \psi = c(x)f(\eta),$$
$$t_0 - t_\infty = d(x). \tag{11}$$

Where K is a constant included in the definition of η merely for convenience. Also for convenience, we define the temperature excess ratio ϕ, as

$$\phi \equiv \frac{t - t_\infty}{t_0 - t_\infty}. \tag{12}$$

Using equations (10)–(12), equations (4)–(9) become

$$f''' + \left(\frac{c_x}{\eta}\right)ff'' - \left(\frac{c_x}{\eta} + \frac{2cb_x}{b\eta}\right)f'^2 - \left(\frac{c_x}{\eta^2}\right)ff'$$
$$- \left(\frac{1}{\eta}\right)f'' + \left(\frac{1}{\eta^2}\right)f' = 0 \tag{13}$$

$$\frac{1}{\sigma}\phi'' + \left(\frac{1}{\sigma\eta}\right)\phi' + \left(\frac{c_x}{\eta}\right)f\phi' - \left(\frac{cd_x}{d\eta}\right)f'\phi = 0 \tag{14}$$

$$f(0) = f'(0) = \phi(0) - 1 = \phi(\infty) = f'(\infty) = 0 \tag{15}$$

$$\int_0^\infty f'^2 \frac{d\eta}{\eta} = JK/2\pi\rho\nu^2c^2b^2 \tag{16}$$

$$\int_0^\infty f'\phi \, d\eta = Q/2\pi c_p \mu c d \tag{17}$$

where σ is the Prandtl number.

Similarity requires f and ϕ to be functions of η alone and this will occur when

$$c_x \equiv C_1 = \text{constant} \tag{18}$$

$$2\frac{cb_x}{b} \equiv C_2 = \text{constant} \tag{19}$$

$$\frac{d_x c}{d} \equiv C_3 \equiv \text{constant}. \tag{20}$$

It is also required that the physical boundary conditions (7) as well as the compatibility conditions (8) and (9) reduce to similarity form. These are written out in current terms in equations (15)–(17). In the appendix, necessary conditions for similarity are determined (in a general way) from equations (18)–(20), and it is shown that similarity exists when both b and d are either power law or exponential in x. For $d = Nx^n$, the power law case, $c = C_1 x$. For the exponential case c = constant. Choosing $C_1 = 1$ for the power law case, it follows from equations (16) and (17) that $C_2 = -2$, and $C_3 = -1$. Then equations (13) and (14) become

$$\left(f'' - \frac{f'}{\eta}\right)' = \frac{ff'}{\eta^2} - \frac{f'^2}{\eta} - \frac{ff''}{\eta} \tag{21}$$

$$(\eta\phi' + \sigma f\phi)' = 0 \tag{22}$$

where: $b(x) \equiv x^{-1}$, $c(x) \equiv x$, $d(x) \equiv Ex^{-1}$; and E can be determined from equation (17). Using $f'(0) = f(0) = 0$, equation (21) can be integrated three times to give

$$f(\eta) = \frac{\eta^2}{A + \frac{1}{4}\eta^2} \tag{23}$$

where A is a constant of integration. Note that (23) satisfies the boundary conditions (15) for all values of A, but A can be determined from (16) to be

$$A = \tfrac{16}{3}\pi\rho\nu^2/JK. \tag{24}$$

For convenience, we now choose

$$K = \tfrac{16}{3}\pi\rho\nu^2/J \tag{25}$$

and then $A = 1$, and equation (23) becomes

$$f(\eta) = \frac{\eta^2}{1 + \frac{1}{4}\eta^2}. \tag{26}$$

Having done this we have Schlichting's [1] results

$$u = \frac{3}{8\pi}\frac{J}{\mu x}(1 + \tfrac{1}{4}\eta^2)^{-2} \tag{27}$$

$$v = \frac{1}{4}\sqrt{\left(\frac{3}{\pi}\right)}\frac{\sqrt{(J/\rho)}}{x}\eta\left[\frac{1 - \frac{1}{4}\eta^2}{(1 + \frac{1}{4}\eta^2)^2}\right] \tag{28}$$

where the similarity variable η is now defined as:

$$\eta = \sqrt{\left(\frac{3}{16\pi}\right)}\frac{\sqrt{(J/\rho)}}{\nu}\frac{y}{x}. \tag{29}$$

Schlichting did not consider thermal transport. By integrating equation (22) and applying the boundary conditions (15) the temperature excess ratio may be shown to be:

$$\phi(\eta) = (1 + \tfrac{1}{4}\eta^2)^{-2\sigma} \tag{30}$$

and then from equation (17) we have

$$t = t_\infty + \frac{(2\sigma + 1)Q}{8\pi\mu c_p x}(1 + \tfrac{1}{4}\eta^2)^{-2\sigma} \tag{31}$$

where

$$E = \frac{2\sigma + 1}{8\pi}\frac{Q}{\mu c_p}. \tag{32}$$

It may be shown that equation (30) is equivalent to that of Squire [6] for sufficiently large Reynolds numbers. Numerical values for the constants J and Q can be determined from known physical conditions at the nozzle. For a uniform velocity distribution across the nozzle

$$J = \frac{\pi\rho v^2}{4} Re_D^2 \tag{33}$$

where

$$Re_D \equiv \frac{U_j D}{\nu} \tag{34}$$

and U_j is the jet velocity at the nozzle. For developed Poiseuille flow at the nozzle

$$J = \frac{\pi\rho v^2}{3} Re_D^2 \tag{35}$$

where the Re_D here is based on the average jet velocity at the nozzle.

Conditions (33) and (35) are the two limiting cases. For convenience we may rewrite these equations using the definition

$$R \equiv \frac{Re_D}{a} \tag{36}$$

where: $a = 8/(\sqrt{3}) = 4{\cdot}62$ implies a flat velocity profile, and $a = 4$ corresponds to a parabolic velocity distribution. Note now that $J = 16\pi\rho\nu^2R^2/3$ and $K = 1/R^2$.

In order to evaluate the constant Q, the temperature distribution at the nozzle must be known. The temperature distribution across the nozzle is independent of the velocity profile and is uniform if the walls are adiabatic. For these conditions, Q is given by the following expression:

$$Q = \frac{kA_j}{D}(t_j - t_\infty)\sigma Re_D \tag{37}$$

for a uniform profile where A_j and t_j are the cross-sectional area and temperature of the jet at the nozzle respectively. Using (34) and (36), the distributions are calculated as:

$$u = \frac{\nu R^2}{x}\frac{f'}{\eta} \tag{38}$$

$$v = \frac{\nu R}{x}\eta\left(\frac{f}{\eta}\right)' \tag{39}$$

$$t - t_\infty = (t_j - t_\infty)\left(\frac{2\sigma + 1}{32}\right)\left(\frac{D}{x}\right)Re_D\phi \tag{40}$$

where

$$f(\eta) = \frac{\eta^2}{1 + \frac{1}{4}\eta^2} \tag{41}$$

$$\phi(\eta) = (1 + \tfrac{1}{4}\eta^2)^{-2\sigma} \tag{42}$$

and

$$\eta = R\frac{y}{x}. \tag{43}$$

The nondimensionalized axial and radial components of the velocity as well as the temperature excess ratio are shown on Fig. 2. Recall

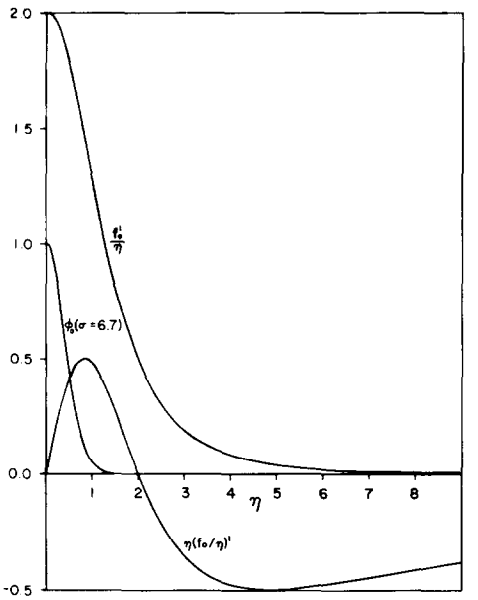

FIG. 2. Unperturbed base flow velocities and temperature for round jet.

that ϕ is dependent on Prandtl number. The curve shown is for $\sigma = 6{\cdot}7$. It is interesting to note that the radial velocity component changes sign at $\eta = 2$ in the boundary layer.

Effects of buoyancy are included by retaining the buoyancy force term in equation (5). This results in the following additional term in equation (13), coupling f and ϕ.

$$K^2\left(\frac{g\beta}{\nu^2}\right)\left(\frac{d}{cb^4}\right)n\phi. \tag{44}$$

Since $d/b^4c = Ex^2$ similarity does not result when thermal buoyancy is included. This suggests a perturbation analysis and a perturbation parameter ε:

$$\varepsilon(x) = K^2\left(\frac{g\beta}{\nu^2}\right)\left(\frac{d}{cb^4}\right). \tag{45}$$

The stream function ψ, and the temperature excess ratio ϕ are written in terms of the perturbation parameter $\varepsilon(x)$ as:

$$\psi(\eta, x) = \psi_0(\eta) + \varepsilon(x)\,\psi_1(\eta) + \ldots \tag{46}$$

$$\phi(\eta, x) = \phi_0(\eta) + \varepsilon(x)\,\phi_1(\eta) + \ldots \tag{47}$$

Note that the perturbation effect of thermal buoyancy may be written variously as:

$$\varepsilon(x) = \frac{256}{9}\pi^2 E \frac{g\beta\mu^2}{J^2} x^2 = \frac{Gr_{x,\Delta t_0}}{R^4} = a^4 \frac{(x/D)^2}{Re_D^2 Fr^2}. \quad (48)$$

In terms of conditions at the nozzle for a flat profile and adiabatic walls upstream

$$\varepsilon(x) = \frac{128}{9}(2\sigma + 1)\frac{Gr_{D,\Delta t_j}}{Re_D^3}\left(\frac{x}{D}\right)^2 \quad (49)$$

where the Grashof and Froude numbers are defined as

$$Gr_{x,\Delta t_0} \equiv \frac{g\beta x^3 \Delta t_0}{\nu^2} \quad (50)$$

$$Gr_{D,\Delta t_j} \equiv \frac{g\beta D^3 \Delta t_j}{\nu^2} \quad (51)$$

$$Fr \equiv U_j/U_c. \quad (52)$$

The jet velocity at the nozzle is U_j and $U_c \equiv \sqrt{[g\beta x(t_0 - t_\infty)]}$ is the "convection" velocity. The resulting expressions for u and v are

$$u = \frac{\nu R^2}{x}[f_0'/\eta + \varepsilon(x) f_1'/\eta + \ldots] \quad (53)$$

$$v = \frac{\nu R}{x}[\eta(f_0/\eta)' + \varepsilon(x)\eta^3(f_1/\eta^3)' + \ldots] \quad (54)$$

where f_0 and ϕ_0 are the solutions of equations (21) and (22). The governing equations for the first perturbations f_1 and ϕ_1 are:

$$[\eta(f_1'/\eta)']' + f_0(f_1'/\eta)' + 3(f_0'/\eta)' f_1 + \eta\phi_0 = 0 \quad (55)$$

$$(\eta\phi_1')' + \sigma(f_0\phi_1' - f_0'\phi_1 + f_1'\phi_0 + 3f_1\phi_0') = 0. \quad (56)$$

It is also necessary to examine the effect of the perturbation on the momentum and heat flux conditions. By using (46) and (47) in (16) and (17) the momentum and heat flux conditions become:

$$J = 2\pi\rho\nu^2 R^2\left[\int_0^\infty f_0'^2 \frac{d\eta}{\eta} + 2\varepsilon\int_0^\infty f_0' f_1' \frac{d\eta}{\eta} + \ldots\right] \quad (57)$$

$$Q = 2\pi\mu c_p(t_0 - t_\infty)x\left[\int_0^\infty \phi_0 f_0' \, d\eta + \varepsilon\int_0^\infty (\phi_0 f_1' + \phi_1 f_0')\, d\eta + \ldots\right] \quad (58)$$

Equation (58) indicates that the inclusion of thermal buoyancy causes the momentum flux to vary with x, as expected. Since there are no sources of heat in the flow field, the second integral in equation (58) must be zero. This integral is shown to be zero by integrating the energy equation (56) from 0 to ∞ and using the following boundary conditions.

$$f_1(0) = f_1'(0) = \phi_1'(0) = f_1'(\infty) = \phi_1(\infty) = 0. \quad (59)$$

Equations (55) and (56), subject to the boundary conditions (59), were solved numerically in the usual fashion of a two-point boundary value problem. Since there are three known boundary conditions at zero and two at infinity, it was desirable to integrate the equations out from $\eta = 0$, to $\eta = \eta_{edge}$. A fourth order predictor-corrector was used to integrate the equations and a conventional correction scheme was employed to change the guessed boundary conditions. It is necessary to have values for the dependent variables and a sufficient number of derivatives thereof at the starting point ($\eta = 0$ here). The value of the highest order derivatives are generally obtained (for problems posed in Cartesian coordinates) by inverting the governing equations. For this case, however, numerical complications arise because of the axisymmetric geometry, since the highest order derivatives are equal to expressions which involve division by various powers of η. To avoid this difficulty, expansions for small values of η were obtained, and the behavior of f_1 and ϕ_1 was determined for values of η near zero to be:

$$f_1(\eta) \sim A\left[1 + \frac{3}{8}\eta^4 - \frac{5}{64}\eta^6\right] + B\left[\left(\eta^2\right.\right.$$

$$+\frac{1}{16}\eta^6\Big)\ln\eta-\frac{1}{8}\eta^4-\frac{5}{192}\eta^6\Big]+C\Big[\eta^2+\frac{1}{16}\eta^6\Big]+\Big[-\frac{1}{16}\eta^4+\Big(\frac{1+\sigma}{192}\Big)\eta^6\Big]+\ldots \tag{60}$$

$$\phi_1(\eta)\sim G\Big[1+\frac{\sigma}{2}\eta^2-\frac{\sigma}{16}\eta^4\Big]+H\Big[\Big(1+\frac{\sigma}{2}\eta^2-\frac{\sigma}{16}\eta^4\Big)\ln\eta-\frac{3\sigma}{4}\eta^2+\Big(\frac{3\sigma-2\sigma^2}{64}\Big)\eta^4\Big]+\Big[-\frac{\sigma C}{2}\eta^2+\frac{\sigma(1+16\sigma C)}{64}\eta^4\Big]+\ldots. \tag{61}$$

From the boundary conditions (59) it can be shown that $A = B = H = 0$.

For completeness, the behavior of f_1 and ϕ_1 was determined for large values of η. For $\sigma \neq n/4$ where $n = 1, 2, 3, 4, \ldots$ we have:

$$f_1(\eta)\sim A'\Big[\frac{1}{48}\eta^2-2\ln\eta-\frac{1}{6}-48\eta^{-2}\ln^2\eta+1452\eta^{-2}\ln\eta\Big]+B'[1+48\eta^{-2}\ln\eta]+C'[\eta^{-2}]+\Big[\frac{-4^{2\sigma}}{16(1-\sigma)(1-2\sigma)(3-2\sigma)}\Big]\eta^{4-4\sigma}+4^{2\sigma-1}\Big[\frac{4\sigma^4-12\sigma^3+13\sigma^2-6\sigma+4}{\sigma(1-\sigma)^2(1-2\sigma)^2(3-2\sigma)}\Big]\eta^{2-4\sigma}+\ldots \tag{62}$$

$$\phi_1(\eta)\sim G'\Big[1+\Big(\frac{8\sigma}{1-2\sigma}\Big)\eta^{-2}+\Big(\frac{16\sigma}{\sigma-1}\Big)\eta^{-4}\Big]+H'\eta^{-4\sigma}\Big[1+8\sigma\Big(\frac{1-2\sigma}{1+2\sigma}\Big)\eta^{-2}+16\sigma\Big(\frac{4\sigma^3-\sigma-1}{(1+\sigma)(1+2\sigma)}\Big)\eta^{-4}\Big]-3\sigma B'4^{2\sigma}\eta^{-4\sigma}\ln\eta+\ldots. \tag{63}$$

It is noted that the character of these expansions for f_1 and ϕ_1 is Prandtl number dependent and logarithmic terms arise for Prandtl numbers that are integral multiples of $\frac{1}{4}$ (i.e. for $\sigma = n/4$ where $n = 1, 2, 3, \ldots$).

The numerical procedure is to guess C and G such that the two distant boundary conditions are satisfied (i.e. $A' = G' = 0$). Note that $2C = f_1''(0) = f_1'/\eta(0) \equiv u_1(0)$ and $G = \phi_1(0)$; $A'/24 = f_1''(\infty) = u_1(\infty)$ and $G' = \phi_1(\infty)$. By using the above procedure, equations (55) and (56) were numerically integrated subject to the boundary conditions (59) for several Prandtl numbers of 6·7, 10 and 20.

RESULTS

The perturbation velocities and temperatures are shown on Figs. 3–5 for Prandtl numbers of 6·7, 10 and 20. Figure 3 shows the axial velocity

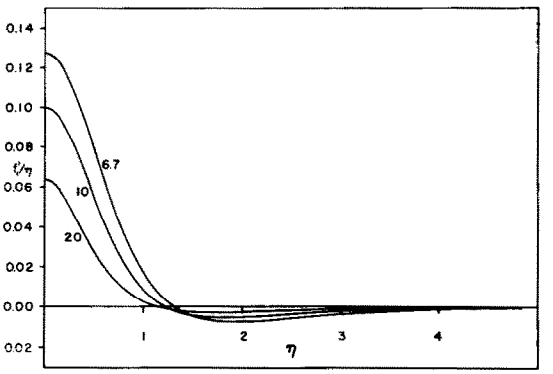

FIG. 3. Axial component of velocity induced by thermal buoyancy.

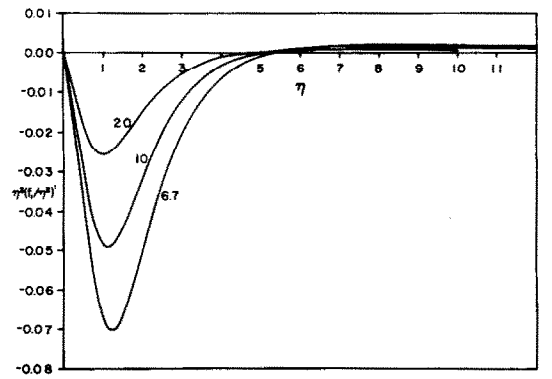

FIG. 4. Radial component of velocity induced by thermal buoyancy.

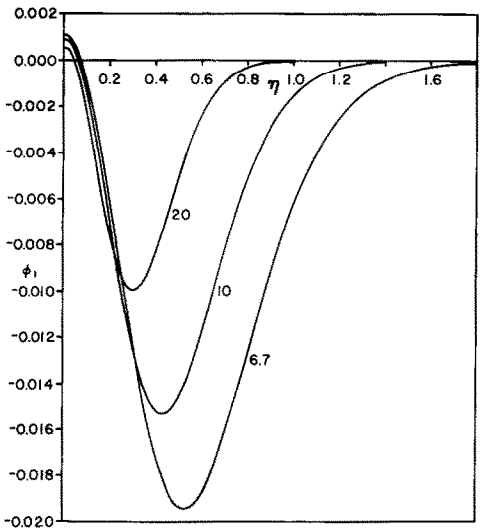

FIG. 5. Temperature perturbation resulting from the inclusion of thermal buoyancy.

component induced by buoyancy. Figures 4 and 5 show the corresponding radial velocity component and the temperature respectively. Composite velocity and temperature distributions

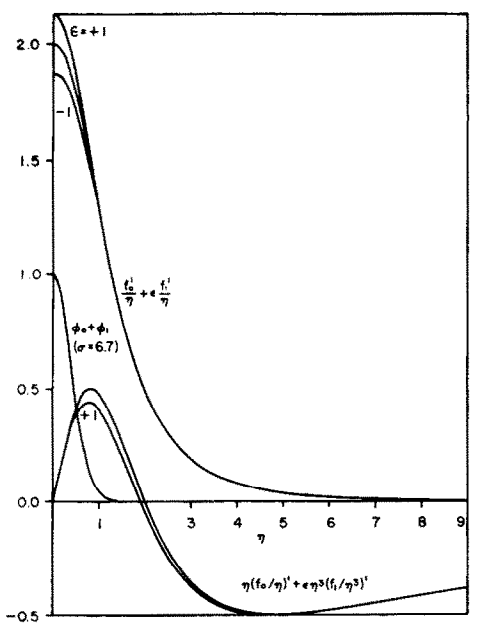

FIG. 6. Composite velocities and temperature distribution for various amounts of thermal buoyancy.

are shown on Fig. 6 for $\varepsilon = \pm 1$. Note that the effect of buoyancy on the temperature distribution is so small for $\varepsilon = 1$ that it cannot be shown using the scales of Fig. 6.

These figures show that the effect of thermal buoyancy on the velocity and temperature profiles increases as the Prandtl number decreases. This is consistent with physical reasoning. The relative thickness of the thermal boundary region increases as the Prandtl number decreases thus increasing the size of the buoyant region. In addition, for a given temperature difference, the magnitude of the total buoyant force is increased as a result of the increased size of the thermal region. Or more concisely, as the Prandtl number decreases, the relative size of the thermal region increases, causing a larger and more extensive thermal buoyancy force. It can also be seen that the effect of thermal buoyancy manifests itself most strongly on the axial velocity component; causing a nearly 7 per cent increase in the centerline velocity for a Prandtl number of 6·7 and $\varepsilon = 1$.

From Fig. 4 it can be seen that the radial velocity component is reduced by about 7 per cent for a Prandtl number of 6·7 and $\varepsilon = 1$. The point of radial velocity reversal is also moved slightly toward the axis by thermal buoyancy. The radial velocity at the edge of the boundary layer is very little affected by thermal buoyancy for the Prandtl numbers considered here.

The effect of buoyancy on the temperature profiles can be determined from the nondimensionalized temperature excess ratio as shown on Fig. 5. Comparing the magnitude of the temperature perturbation to the velocity perturbation we see that the temperature profiles are affected least by the inclusion of thermal buoyancy. The temperature corrections occur near the center of the jet ($\eta \leqslant 2$); and slightly increase the centerline temperature. However, they reduce the temperature profile by less than 2 per cent at larger η.

A striking feature of the profiles shown in Figs. 3–5, is that the curves exhibit negative portions suggesting a reverse effect on velocity

and temperature at a certain point in the boundary layer. We see from Fig. 6 that the composite solutions for the axial velocity and the temperature excess ratio are everywhere positive (even for the extreme cases $\varepsilon = \pm 1$). This "reversal" behavior can be explained by considering the effects of buoyancy on the physics of the velocity and temperature fields.

That the buoyancy coupling would increase the axial velocity in the region of the thermal boundary layer is expected. The increased axial velocity causes the magnitude of the negative (inward) radial velocity to increase in the vicinity of the edge of the thermal boundary layer. In fact, from Fig. 4 it can be seen that the perturbation radial velocity component reaches a maximum near the edge of the thermal boundary layer. It is this increase in the inward portion of the radial component which thins, or squeezes in, the axial velocity distribution just beyond the edge of the thermal boundary layer.

It is interesting that McNaughton and Sinclair [9] observed such a thinning in their experimental jet studies as a result of small density differences between the jet fluid and that of the surrounding medium.

The alteration of the temperature field, however, appears to be caused by more complicated interactions since the positive radial velocity component is reduced inside the region of the thermal boundary layer because of the increased axial component in that region. In fact, it can be seen that the effect of buoyancy on the radial velocity component is larger inside the thermal region than outside it. This effect alone would tend to "thicken" the temperature profile. There is, however, another effect. The concept of "turning on" an aiding thermal buoyancy force (i.e. letting ε take on positive, nonzero values) is equivalent to an effective increase in the center-line temperature. This accounts for the slight positive portion of Fig. 5. At the same time, however, the increased axial velocity causes the quantity of heat convected downstream to increase without an associated increase in the heat diffused outward. Also the heat convected outward is reduced because of the lower radial velocity. The net result is, then, that there is a relative concentration (toward the axis) of heat convected downstream with buoyancy forces present. This would tend to cool or "thin" the temperature profile. Apparently the "thinning" of the temperature profile is slightly more effective than the thickening caused by altered radial velocity. This would explain the mild "thinning" of the temperature profile.

The mass rate of flow, $\dot{m}$ of the jet can be calculated as

$$\dot{m} = 8\pi\mu x\left[1 + \varepsilon(x)\frac{f_1(\infty)}{4} + \ldots\right]. \quad (64)$$

Thus, the buoyancy effect introduces an additional x^3 dependence of $\dot{m}$. Values of $f_1(\infty)$, $f_1''(0)$ and $\phi_1(0)$ are presented in Table 1. Since

Table 1

σ	$f_1(\infty)$	$f_1''(0)$	$\phi_1(0)$
6·7	−0·006553	0·1273	0·001113
10	−0·004328	0·09977	0·0008991
20	−0·002340	0·06365	0·0005535

$f_1(\infty)$ is negative, the effect of buoyancy decreases the mass flow rate. The magnitude of $f_1(\infty)$ indicates however that this effect is small. From Fig. 3 it might appear that the mass flow should be increased because of the dominant increase in the axial velocity. However, since the cross-sectional area varies as the square of the radial distance; even small changes in the velocity profile further from the center can become significantly important in the mass flow integral. This is the case for the profiles of Fig. 3.

Although the inclusion of thermal buoyancy effects does not produce extreme changes in the velocity and temperature fields, it is noted that the effects on the velocity field increase as the Prandtl number decreases.

We note that the opposed buoyancy effect is included in these results with $\varepsilon < 0$.

Since thermal buoyancy is seen above to result in rather small changes in the velocity and

temperature fields, it may not be feasible to experimentally verify these predictions. Nevertheless, even these small effects of buoyancy coupling could have important influences on the hydrodynamic stability of jet flows. The effect on stability might be particularly strong when the buoyant force opposed the jet momentum, and, for Prandtl numbers which concentrate this retardation of flow near the center of the jet. Because of the large difference between laminar and turbulent transport parameters, entrainment, etc., it is of considerable practical importance to know under what conditions one might expect each of these flow regimes.

The present results indicate that small amounts of buoyancy change the transport characteristics of a jet, and show the trends for potentially larger amounts of thermal buoyancy. These results also provide a basis for calculating the effects of buoyancy on the hydrodynamic stability of laminar jets.

ACKNOWLEDGEMENTS

The writers wish to acknowledge support for this research under the National Science Foundation Grant GK18529.

REFERENCES

1. H. SCHLICHTING, Laminare Strahlausbreitung, *ZAMM* **13**, 260; *Boundary Layer Theory*, pp. 164, 181. McGraw-Hill (1933).
2. W. BICKLEY, The plane jet, *Phil. Mag.* **23**, 727 (1937).
3. E. N. ANDRADE and H. S. TSIEN, The velocity-distribution in a liquid-into-liquid jet, *Proc. Phys. Soc.* **49**, 381 (1937).
4. W. N. ANDRADE, The velocity distribution in a liquid-into-liquid jet, Part 2: The plane jet, *Proc. Phys. Soc.* **51**, 784 (1939).
5. L. LANDAU, See L. D. LANDAU and E. M. LIFSHITZ, *Fluid Mechanics*, p. 86. Pergamon Press, Oxford (1943).
6. H. B. SQUIRE, The round laminar jet, *Q. J. Mech. Appl. Math.* **4**, 321 (1951).
7. R. S. BRAND and F. J. LAHEY, The heated laminar vertical jet, *J. Fluid Mech.* **29**, 305 (1967).
8. M. VIGNES, Contribution à l'étude des jets gazeux verticaux dans une atmosphère calme, *Rev. Gén. Thermique* **VII**, 1205 (1968).
9. K. J. MCNAUGHTON and C. G. SINCLAIR, Submerged jets in short cylindrical flow vessels, *J. Fluid Mech.* **25**, 367 (1966).
10. G. F. MARSTERS, Some observations on the transition to turbulence in small, unconfined free jets, Report #1–69, Queen's University, Kingston, Ontario, Canada (1969).
11. C. P. MCKENZIE and D. B. WALL, Transition from laminar to turbulence in submerged and bounded jets, *Fluidics Q.* **4**, 38 (1968).

APPENDIX

Necessary Conditions for Similarity of the Boundary-Layer Equations

Recall that the boundary-layer equations in cylindrical coordinates admit similarity form if equations (18)–(20) are satisfied. By integrating equation (18) we arrive at

$$c(x) = C_1 x + C_4. \tag{A.1}$$

Using equation (A.1) and integrating equation (19) $b(x)$ is found to be

$$b(x) = C_5(C_1 x + C_4)^{C_2/2C_1}. \tag{A.2}$$

Then from equation (20) get

$$d(x) = C_6(C_1 x + C_4)^{C_3/C_1}. \tag{A.3}$$

Note that equations (A.2) and (A.3) are valid for $C_1 \neq 0$. If $C_1 = 0$ equation (A.1) becomes

$$c(x) = C_4 \tag{A.4}$$

and from equations (19) and (20)

$$b(x) = C_5 e^{(C_2/2C_4)x} \tag{A.5}$$

and

$$d(x) = C_6 e^{(C_3/C_4)x}. \tag{A.6}$$

We see that both the power law and exponential centerline temperature distributions result in similarity. A completely analogous analysis yields the same results for the two-dimensional case. Note however that for either case the boundary conditions must be able to be put in similarity form.

EFFET D'ARCHIMEDE DANS DES JETS CIRCULAIRES LAMINAIRES ET VERTICAUX

Résumé—On a mené une analyse de perturbation qui englobe l'effet d'Archimède et son action sur les champs de vitesse et de température d'un jet rond laminaire et vertical. Une solution numérique des équations de perturbation montre que l'effet prédominant de la poussée thermique positive est d'accroître la composante axiale de la vitesse du jet. On montre que l'importance de l'effet croît lorsque le nombre de

Prandtl diminue. D'autres détails de l'effet d'Archimède sur les champs dynamique et thermique sont présentés et discutés. On s'attend à ce que l'effet d'Archimède puisse avoir un grand rôle sur la stabilité laminaire.

THERMISCHER AUFTRIEB IN RUNDEN, LAMINAREN, VERTIKALEN DÜSENSTROMUNGEN

Zusammenfassung—Eine Störungsrechnung wurde durchgeführt, die die Auswirkung eines geringen thermischen Auftriebs auf die Geschwindigkeits- und Temperaturfelder einer runden, laminaren, vertikalen Düsenströmung berücksichtigt. Eine numerische Lösung der sich daraus ergebenden Störungsgleichung seigt, dass durch den überwiegenden Effekt des positiven thermischen Auftriebs die axiale Geschwindigkeitskomponente der Düsenströmung anwächst. Es wird gezeigt, dass der Effekt mit fallender Prandtl–Zahl grösser wird. Andere Einzelheiten von Auftriebseffekten auf die Strömungs- und Temperaturfelder werden dargestellt und diskutiert. Es wird vermutet, dass Auftriebseffekte einen grossen Einfluss auf die laminare Stabilität ausüben.

ТЕРМИЧЕСКАЯ ПОДЪЕМНАЯ СИЛА В КРУГЛЫХ ЛАМИНАРНЫХ ВЕРТИКАЛЬНЫХ СТРУЯХ

Аннотация—Проведено исследование возмущенного движения, в котором учитывается незначительное влияние термической подъемной силы на поле скоростей и температур в круглой вертикальной ламинарной струе. Численное решение полученных уравнений возмущения показывает, что преобладающее влияние положительной термической подъемной силы увеличивает продольную составляющую скорости струи. Показано, что это влияние возрастает при уменьшении значений числа Прандтля. Показаны и обсуждаются другие стороны влияния этой силы на поля скоростей и температур. Ожидается, что свободная конвекция может оказывать брльшое влияние на устойчивость ламинарного течения.